JMEPEG (2005) 14:448-459
DOI: 10.1361/105994905X56223

1059-9495/$19.00

Nanostructured Component Fabrication by Electron Beam-Physical Vapor Deposition

Jogender Singh and Douglas E. Wolfe

(Submitted April 27, 2005; in revised form May 12, 2005)

Fabrication of cost-effective, nano-grained net-shaped components has brought considerable interest to Department of Defense, National Aeronautics and Space Administration, and Department of Energy. The objective of this paper is to demonstrate the versatility of electron beam-physical vapor deposition (EB-PVD) technology in engineering new nanostructured materials with controlled microstructure and microchemistry in the form of coatings and net-shaped components for many applications including the space, turbine, optical, biomedical, and auto industries. Coatings are often applied on components to extend their performance and life under severe environmental conditions including thermal, corrosion, wear, and oxidation. Performance and properties of the coatings depend upon their composition, microstructure, and deposition condition. Simultaneous co-evaporation of multiple ingots of different compositions in the high energy EB-PVD chamber has brought considerable interest in the architecture of functional graded coatings, nano-laminated coatings, and design of new structural materials that could not be produced economically by conventional methods. In addition, high evaporation and condensate rates allowed fabricating precision net-shaped components with nanograined microstructure for various applications. Using EB-PVD, nano-grained rhenium (Re) coatings and net-shaped components with tailored microstructure and properties were fabricated in the form of tubes, plates, and Re-coated spherical graphite cores. This paper will also present the results of various metallic and ceramic coatings including chromium, titanium carbide (TiC), titanium diboride (TiB_2), hafnium nitride (HfN), titanium-boron-carbonitride (TiBCN), and partially yttria stabilized zirconia (YSZ) TBC coatings deposited by EB-PVD for various applications.

Keywords electron beam physical vapor depositon, function graded materials, nanostructure, Rhenium, TiBCN, yttria stabilized zirconia

I. Introduction

Coatings play an important role ranging from undersea to space applications, including communications, sensors, satellites, optics, auto, and aerospace industries (Ref 1-5). High-temperature components of gas-turbine engines for aircraft such as airfoils and vanes are coated with metallic and ceramic coatings to enhance performance and reliability (Ref 6-9). Thus, there is a continuous effort to engineer surface properties of the material, enhancing the life of components under severe environmental conditions where corrosion, high-temperature oxidation, and wear are concerns. Similarly, multilayered ceramic and metallic films are extensively used in the fabrication of microelectronic and communication components (Ref 10). It is important to understand the interrelationship of applications, coatings, and processes. Applications dictate the selection of coating materials, and the desired thermal, chemical, and mechanical properties often determine the deposition method and processing parameters (Ref 11).

Coating processes can be broadly classified into three groups: vapor phase, which includes physical vapor deposition (PVD) and chemical vapor deposition (CVD); liquid phase, which includes painting, dipping, and electroplating; and solid phase, which includes plasma spray processes and laser cladding (Ref 12-17). Each process can again be subclassified based on the source of energy used for the deposition of coatings. Each of these processes has its advantages and disadvantages. Comparison of CVD, PVD, and plasma spray processes is given in Table 1 (Ref 18-20). Chemical and physical conditions during the deposition reaction can strongly affect the composition, residual stresses, and microstructure (i.e., amorphous, polycrystalline, epitaxial, and textured) of the coating. The desired coating thickness and material properties (including microstructure, physical, and mechanical properties) are dictated by its application, which will determine the coating deposition process to be used.

2. Electron Beam-Physical Vapor Deposition Process

Electron beam-physical vapor deposition (EB-PVD) is a simple process in which a focused high-energy electron beam is directed to melt the evaporant material(s) in a vacuum chamber (Fig. 1a). The evaporating material condenses on the surface of the substrates or components resulting in the formation of deposit, i.e., coating. During deposition, external heating is often applied to the substrate for enhancing metallurgical bonding between the coating and the substrate. EB-PVD is primarily

This paper was presented at the International Symposium on Manufacturing, Properties, and Applications of Nanocrystalline Materials sponsored by the ASM International Nanotechnology Task Force and TMS Powder Materials Committee, October 18-20, 2004, Columbus, OH.

Jogender Singh and **Douglas E. Wolfe,** Applied Research Laboratory, Penn State University, University Park, PA 16804. Contact e-mail: dew125@psu.edu.

Table 1 Comparison between CVD, PVD, EB-PVD, and plasma spray processes (Ref 18-20)

Coating process	Substrate temperature, °C	Deposition rate	Surface roughness	Type of bonding	Typical microstructure	Coating material	Environment	Flexible
Plasma spray	RT to 800 (flexible)	>100 μm/min	Very rough	Mechanical	Deformed lamella	Metal, ceramic	Noise	Flexible
CVD	>800-1200 (must)	<0.08 μm/min (<5 μm/h)	Smooth	Diffusional	Columnar, equiaxed	Metal, ceramic	Chemical gas disposal	Limited
PVD sputtering	<600 (flexible)	<0.08 μm/h)	Smooth	Diffusional	Columnar	Metal, ceramic	Clean	Limited
EB-PVD	RT to 1200 (flexible)	0.01 to 100 μm/min	Smooth	Diffusional	Columnar, equiaxed	Metal, ceramic	Clean	Flexible

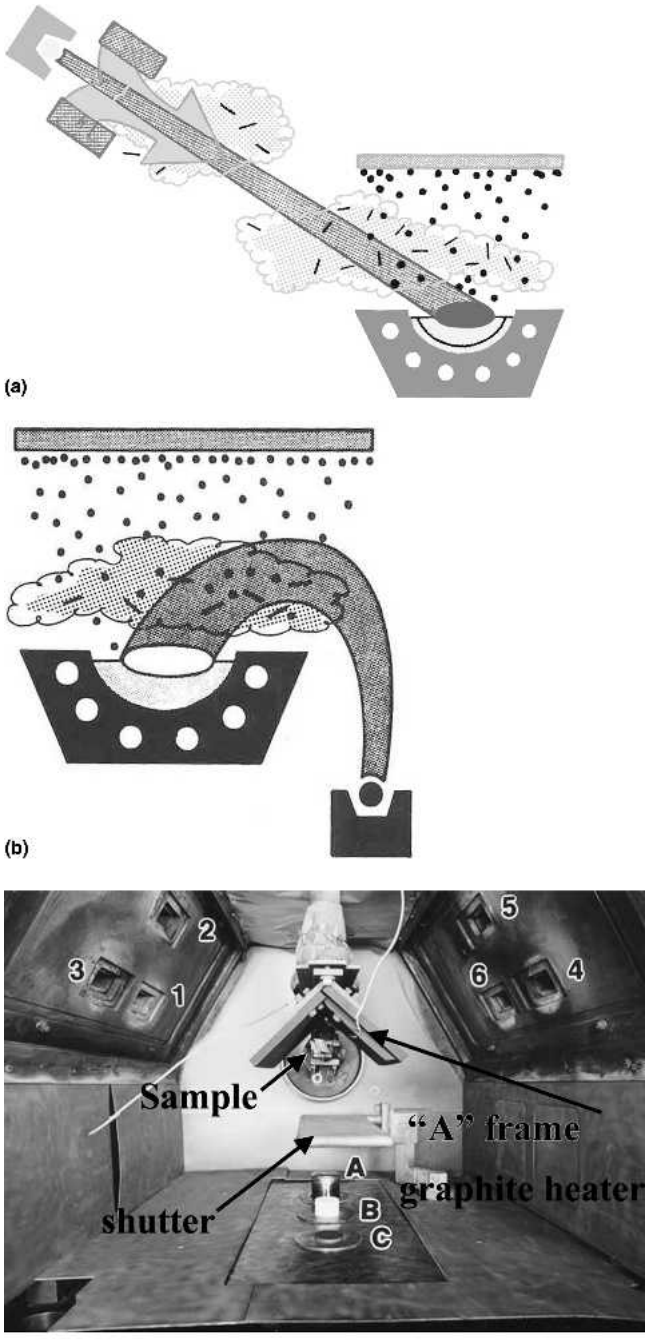

Fig. 1 Schematic diagram showing (a) straight, (b) 90° electromagnetic deflected electron beam, and (c) EB-PVD chamber showing six EB guns (1-6), three continuous ingot (A-C) feeding system, an "A-shaped" graphite heater, deposition shutter, and rotating sample.

a line-of-sight process; therefore, uniform coating of complex parts (such as turbine airfoils) is accomplished by continuous rotation in the vapor cloud during the deposition process.

There are four main components in the EB-PVD unit, namely, electron-beam (EB) gun assembly, water cooled copper crucible, which contains the material to be evaporated, the substrate (part to be coated), and the vacuum chamber unit with enhanced flexibility for a variety of coating applications. The EB gun can be self-accelerated straight or electromagnetic deflected through 180° or 270°, as shown in Fig. 1(a) and (b). Similarly, the evaporant material is placed in a water-cooled copper crucible, which could be either pocket type for small quantity evaporation application (Fig. 1) or continuous ingot feeding through a copper-cooled crucible (Fig. 1c as marked A, B, and C) for larger quantity evaporation. Flexibility in the application of EB-PVD unit can be enhanced by using many EB guns and continuous multiple ingots feeding system (Fig. 1c).

The industrial research pilot plant scale EB-PVD in the author's laboratory at Penn State University has six electron beam guns, four of which can be used to evaporate the coating material and two of which can be used to preheat the substrate (either directly or indirectly) to facilitate coating adhesion, proper chemistry, and microstructural control (Fig. 1c). Each gun has an average power 45 kW capacity (with peak power 60 kW). The chamber accommodates up to three ingots ranging in size from 25 to 68 mm in diameter and up to 450 mm length. The overall volume of the coating chamber is approximately 1 m^3. The maximum diameter of the substrate with vertical rotation is about 400 mm and can be rotated at a speed of 5.5-110 rpm with a maximum load capacity of 100 kg. The unit also has a horizontal sample holder with a three-axis part manipulator: two rotary axes of 0-14 rpm and a 0-4000 mm/min translation axis. It can accommodate samples weighing up to 20 kg.

The EB-PVD process offers extensive possibilities for controlling variations in the structure and composition of the processed materials. For example, coating compositions can be varied continuously, in the so-called functional graded coatings (FGC). Coatings can be graded from metallic-to-metallic, ceramic-to-ceramic, metallic-to-ceramic, or ceramic-to-metallic depending on what is desired (Ref 21, 22). Also, multilayer coatings composed of alternating layers of different compositions including metals, ceramics, and polymers can be made on a variety of substrates, depending on the desired application (Ref 23, 24). The EB-PVD process offers many desirable characteristics such as relatively high deposition rates (up to 150 μm/min with an evaporation rate of ~10-15 kg/h), dense coatings, controlled composition, tailored microstructure, low contamination, and flexible deposition parameters (Ref 22, 23). The microstructure and composition of the coating can be easily altered by manipulating the process parameters and ingot

compositions. Thus, multilayered ceramic/metallic coatings can be readily formed, and various metallic and ceramic coatings (oxides, carbides, and nitrides) can be deposited at relatively low temperatures. Even elements with low vapor pressure such as Mo, W, Re, and C are readily evaporated by this process. The attachment of the ion beam source to the EB-PVD unit offers two additional features. The substrate surface can be ion beam sputter cleaned/etched prior to deposition to promote adhesion between the coating and the substrate or during deposition to produce the desired microstructure and chemistry as discussed briefly below (Ref 25-29).

2.1 Ion Beam Etching and Precleaning

The function of ion beam etching or precleaning the substrate is the same. In ion beam etching, an ionized beam of gas is directed towards the substrate's surface, prior to deposition, to remove contamination material. This removal of surface material is the result of physical sputtering of the material from the surface due to the momentum transfer between the energetic beam atoms and the substrate surface atoms. Generally, for physical sputtering, an inert gas, such as argon, is used. Bombardment of the substrate surface prior to deposition (i.e., sputter cleaning) promotes better adhesion. The two major effects occurring during this precleaning step are: (a) removal of adsorbed hydrocarbons and water molecules and (b) increasing the density of nucleation sites for condensation (Ref 28). Not removing these materials/molecules prior to deposition results in poor adhesion as they serve as weak links for bonding. Thus, in situ ion beam cleaning of samples prior to coating deposition is often used during these efforts.

2.2 Microstructure and Property Enhancement

In the last several years, ion beams have gained increased importance during the deposition process to enhance the properties of the depositing film. Ion bombardment of the substrate occurs, whereas the source material is evaporated by either resistance or EB. The state of the internal stresses developed in the coating can be changed from tensile to compressive stress by the forcible injection of high-energy atoms (i.e., ion implantation). Thus the ability to control the stress level is an additional feature of the ion-beam-assisted deposition (IBAD) process (Ref 29-33). Chemical vapor deposited coatings generally form with tensile stresses due to the thermal expansion mismatch with the substrate, which often limit the coating thickness before spallation occurs. Ion bombardment during deposition has a tendency to reduce the tensile stress and often changes the intrinsic stress from tensile to compressive. Depending on the energy of the ion beam, texturing or preferred crystal growth orientation can be controlled (Ref 34-36). IBAD can be used to change optical properties and decrease the permeability of water by increasing the density of the deposited film. Changes in the crystal structure of the film have also been reported with IBAD. For example, the microstructure of ZrO_2 was changed from amorphous to polycrystalline using IBAD (Ref 37). In addition, the morphology of molybdenum films deposited on silicon were shown to change from columnar to isotropic due to ion bombardment (Ref 38). In addition, numerous authors have reported increases in the average hardness of coatings deposited with IBAD (Ref 23, 28, 39). The increase in hardness is obtained by increasing the density, decreasing grain size, changing stress state, and controlling the crystallographic texture of the coating. Improved step coverage (i.e., high surface roughness or complex geometries) has also been reported when using IBAD. This is most likely the result of increased atom mobility under bombardment. In addition, ion beams are used in synthesizing coatings by reacting the evaporant with the ionized reactive gases including nitrogen, oxygen, methane, and acetylene. Ionized gas chemically reacts with the vapor cloud, forming alloyed coatings such as nitrides of Hf, Ti, Zr; carbides of Ti, Hf, Ta, and Zr, and oxides of Zr and Al. The choice of the deposition technique is determined by the application for the coating, the desired coating properties, temperature limitation of the substrate, uniformity or consistency of the process, and its compatibility with subsequent processing steps. Chemical and physical conditions during the deposition reaction can strongly affect the resultant microstructure of the coating (i.e., single-crystalline, polycrystalline, amorphous, epitaxial).

3. Applications of the EB-PVD Process

EB-PVD is a derivative of the EB melting technique. Perhaps the most consequential growth phase in EB technology began in the early 1980s and is still in progress. This significant progress was driven by three factors: (a) greatly improved vacuum generation technology, (b) significant advancement in computers, and (c) availability of high quality EB-guns. EB technology was developed for a wide range of applications including surface treatment, welding, glazing, and evaporation for coatings. Incorporation of an ion source in the EB-PVD chamber with multiple ingots has increased its versatility in developing new materials with a very wide range of applications such as the microelectronics, sensors, optics, aerospace, and bio-medical industries. Some successful applications of the EB-PVD and ion beam-assisted EB-PVD processes are given below.

3.1 Superhard Coatings for Machining Tools and Forging Die Industries

Metallic borides, carbides, nitrides, and oxides have been known to be very hard and wear-resistant materials. Applying these hard coatings to cutting tools and inserts can increase their life by several hundred percent (400–600%), reducing costs associated with tool procurement, set-up time, and machine down time. Wear-resistant coatings are often characterized as having high melting temperatures as well as high hardness values. Performance of the coating depends on many factors including structural, chemical, and thermal stability, metallurgical bonding, and machining conditions. All these factors depend upon the process selected for applying the coatings along with its microstructural characteristics including grain size, degree of texture, and density. Most wear-resistant coatings are applied by either CVD or PVD sputtering with typical coating thickness between 2 and 6 μm.

The first wear-resistant coatings, primarily monolithic films of transition metal-nitrides and carbides, were commercially applied by the CVD process, but today they are applied by both CVD and PVD (Ref 40). However, there are two main challenges in the CVD process. First, CVD is a high-temperature deposition process (>800–1200 °C), and thus, coating temperature-sensitive substrates is limited. Second, hazardous chemical gases are often produced during the CVD coating deposition

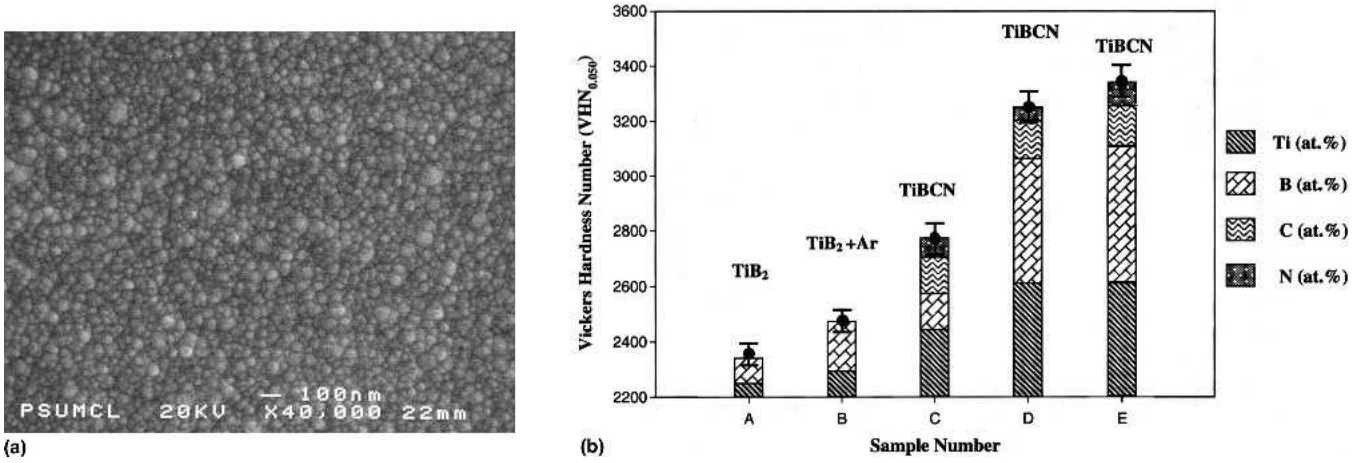

Fig. 2 (a) SEM micrographs showing nano-grained TiB_{2-x} coatings and (b) average Vickers hardness number (VHN) for TiB_2 and TIBCN coatings deposited on WC-6 wt.%Co-0.3 wt.%TaC by argon/nitrogen ion-beam-assisted co-evaporation by EB-PVD.

process and may present environmental concerns. In contrast, PVD coatings are deposited below 500 °C and are more environmentally friendly as hazardous chemical gases are not produced. For the last few years, the trend in applying wear-resistant coatings has changed from single layer to multilayers coatings (typically composed of TiN/AlN, TiN/TiC/TiN, TiN/CrN, and TiN/NbN) that offer superior performance during machining (Ref 41). Research effort is underway in different laboratories to develop new hard materials including TiBCN (Ref 42).

3.2 TiB_2 Coatings Formation by Direct Evaporation

Often, direct evaporation of multicomponent materials results in fractionation. In the case of direct electron beam evaporation of TiB_2 a TiB_{2-x} coating was produced with a hardness of 2940 $VHN_{0.050}$ (Ref 23, 24). The hardness of the coating was increased to 3040 $VHN_{0.050}$ by argon ion-beam-assisted deposition. This was further increased to 3340 $VHN_{0.050}$ by applying a negative bias and bombarding the TiB_{2-x} growing film with argon ions during deposition. The resulting surface morphology shows a uniform, fine-grained surface with an average grain size of less than 100 nm as shown in Fig. 2(a). One of the main challenges in the direct evaporation of TiB_2 is the loss of B due to fractionation (dissociation of Ti and B) resulting in nonuniform stoichiometric composition, i.e., TiB_{2-x}. The loss of boron can be compensated by introducing boron tetrachloride gas into the evaporation chamber during deposition. Unfortunately, boron tetrachloride is colorless, odorless and poisonous, which causes safety issues. Instead, the TiB_2 pool was enriched with boron metal to account for the loss of B from TiB_2 fractionation.

3.3 TiBCN

Very limited research has been conducted in producing TiBCN by using ion-beam-assisted EB-PVD. This section will demonstrate the application of EB-PVD in engineering new coating materials for cutting tool industries applied in a cost effective and environmentally friendly manner. Hard coatings such as TiN, TiC, HfC, ZrC, TiB_2, and TiBCN have been produced by ion beam-assisted EB-PVD at relatively low temperatures (Ref 23, 42-44). Metallic-nitride coatings were produced by evaporating target materials (such as Ti, Zr, Hf) and reacted with ionized nitrogen gas resulting in nitride coatings (RIBA, EB-PVD). Metallic carbides are easy to produce by coevaporation of two target materials: metallic (such as Ti) and graphite in the EB-PVD chamber. Graphite is difficult to evaporate as it sublimes. This challenge has been addressed by indirectly evaporating graphite using a molten pool of tungsten (W) above the graphite target material C(W) (Ref 42). A novel approach was developed in forming TiBCN. Three ingots Ti, TiB_2 and C(W) were coevaporated simultaneously (Ref 42). During the evaporation, nitrogen/argon gas mixture was introduced through the ion source. The ionized nitrogen gas was reacted with the Ti, TiB_2, and C(W) forming TiBCN super hard coatings. The loss of B was compensated by incorporating C and N into TiB_{2-x} resulting in TiBCN. Average hardness of TiBCN as function of the atomic fraction of B, C, and N is given in Fig. 2(b).

3.4 Nano Modulated Thermal Barrier Coatings for the Turbine Industry

There is a continuous two-fold thrust within the Department of Defense (DOD) and commercial turbine industry (including land based and aerospace) to double the thrust-to-weight ratio and extend the life and performance of turbine components under severe environmental conditions including erosion, oxidation, and corrosion. Turbine components are generally made of nickel-based super alloys. The life of turbine components is increased by applying oxidation-resistant coatings composed of platinum-aluminide (Pt–Al) or MCrAlY alloys (M = Ni, Co, Fe, or mixed combination) beneath a thermal barrier coating (TBC) composed of yttria stabilized zirconia, i.e., ZrO_2–8wt.% Y_2O_3 (8YSZ), which is an ideal candidate for thermal protection coatings due to its low density, low thermal conductivity, high melting point, good thermal shock resistance, and excellent erosion resistant properties. 8YSZ has gained widespread acceptance as a TBC material for turbine applications and is generally applied by either plasma spray or EB-PVD processes (Ref 45-48).

TBC applied by EB-PVD process provides advantages over the plasma spray process that includes better strain tolerance, erosion-resistance, bond strength, and surface roughness despite the disadvantage of slightly higher initial thermal con-

ductivity (Ref 49-50). In thermally sprayed TBC, typical grain size is approximately 1-2 μm, and the coating microstructure is associated with intersplat boundary porosity, unmelted, partially melted particles, and microcracks (Ref 51). In EB-PVD, TBC grain sizes vary from 1 to 2 μm near the bond coating/TBC interface, whereas the TBC columnar grain length is often 100-250 μm in thickness with a high degree of crystallographic texture. Keeping the total thickness of the TBC constant, the alignment of the intersplat boundaries with typical spacing of 1-10 μm in the case of thermally sprayed coatings with voids, microcracks have a more pronounced effect on lowering the thermal conductivity than with EB-PVD. The initial thermal conductivity of thermally sprayed 8YSZ is 0.7-0.9 W/m-K, which is lower than the bulk theoretical values 2.2-2.6 W/m-K (Ref 50). However, within the first few hours of turbine engine operation, the thermal conductivity of plasma-sprayed TBC can increase to 1.5 W/m K due to high-temperature sintering effects.

The intersplat/microcracks/porosity provides initial low conductivity for the plasma-sprayed coatings mainly because they are involved with air gaps—air is a better thermal insulator compared with zirconia (air has lower thermal conductivity)—not due to the reduced mean free path for photons/phonon (Ref 50). In addition, the splat boundaries are probably few compared with grain boundaries in producing a significant phonon scattering effect. Nevertheless, the intersplat porosity and boundaries are more effective in reducing the thermal conductivity of the material than the columnar porosity in EB-PVD coatings due to the increased thermal resistance and phonon scattering in the heat conduction direction. If, heat resistance and greater phonon scattering associated with the plasma sprayed TBC microstructure could be applied to TBC produced by EB-PVD, it could make a significant contribution to the reduction of the thermal conductivity. In addition, radiative heat transport becomes increasingly important at high temperatures, so producing a TBC microstructure that also increases infrared (IR) photon scattering will help decrease heat transport through the TBC at high temperatures. Thus, a modified microstructure of the EB-PVD TBC appears to be a very promising method in lowering the thermal conductivity of the coating. Very limited research has been conducted in this area, which could significantly impact the turbine industry by producing TBC materials with lower thermal conductivity for high-temperature applications. It is important to distinguish the effects of phonon scattering, which decreases thermal conductivity, and photon scattering, which reduces radiative heat transport. Both scattering properties are influenced by the presence of interfaces including voids, microporosity, and grain boundaries; however, phonon scattering is affected by dimension features smaller than IR photon scattering. Combination of layering at the micron level and introduction of density changes from layer to layer will significantly reduce the thermal conductivity of the coating. As mentioned earlier, layered periodicity in the coating will significantly reduce both phonon scattering and photon transport. Periodic interfaces and microporosity in the TBC were produced by two approaches. The first approach used was to periodically interrupt the continuous vapor flux by translating the sample away from the vapor cloud for a short period (30-60 s) and then reintroducing the samples into the vapor cloud. During this interruption, the temperature of the sample decreased from ~1000 to ~750 °C. Due to the combination of discontinuous condensation and thermal fluctuations of the sample's surface temperature during this "in and out" method, new grain formation occurs (similar concept as with intersplat boundaries in plasma sprayed TBC).

The second approach used was to periodically interrupt the continuous flux of the vapor cloud by using a "shutter" mechanism. It is important to mention here that the temperature of the substrate remained constant during the deposition process (whereas it decreased to ~750 °C during the "in and out" method"), but discontinuous vapor condensation still occurred. During this interruption period, it is believed that the surface mobility of the condensed species contributes towards surface relaxation. As the vapor flux is prevented from condensing on the surface, the surface atoms with high surface energy and mobility have more time to diffuse to regions of lower surface energy. The periodic relaxation and deposition will contribute in forming layered materials with localized compositional fluctuations having different elastic strains, refractive index, and defect density. Periodicity of such microstructural modifications will have an impact on the thermal conductivity [discussed elsewhere (Ref 51, 52)] and thermal reflectance. In addition to decreasing thermal conductivity, the diffuse interfaces with microporosity should also affect the hemispherical reflectance of the coating and therefore reduce radiative heat transport through the TBC. This suggests that more heat will be reflected from the coatings as the number of layers increases within the TBC. It has been found that there is an additional benefit of interrupting coating deposition by the shutter method. The TBC with diffused layers offered more strain tolerance than that with the single layer. In addition, thermal cycling data clearly shows that the life of TBC coated buttons increased with an increasing number of diffuse layers, with the 20-layer coating showing a 185% improvement (Ref 52). Thus, the overall benefit of the TBC produced by shutter method is three-fold: lower thermal conductivity (25-30%), enhanced thermal reflectance (15-20%), and enhanced strain tolerance with improved thermal cyclic life (180%) depending upon the layer periodicity (Ref 51, 52). Reflectance of the layered TBC produced by "in and out" was increased from ~40% to 55% as the total number of sharp interfaces increased from 10 to 40 at 1 μm wavelength. However, the layered TBC prematurely failed and exhibited limited thermal cyclic life due to the presence of sharp interfaces, which introduced more residual stresses.

3.5 High Reflective Thermal Barrier Coatings

To obtain a high value of reflectance in the multilayer coatings, a stack of alternate layers of high refractive index and low refractive index materials is used. Typically, the refractive index (n) of ceramic TBC materials is ZrO_2 (2.10), CeO_2 (2.35), HfO_2 (1.98), Al_2O_3 (1.60), SiO_2 (1.95), Y_2O_3 (1.82). Similarly, refractive index of monolithic materials can be changed by forming alternate layers of high and low density structures, i.e., modulated microstructure with density variation. The advantage of inhomogeneous antireflection coatings is that they are not sensitive to the angle of incidence. By controlling the thickness of each layer, reflectance of the coating can be controlled over a wide wavelength range. This concept was demonstrated using two materials of different composition and refractive index, as described below.

Multilayer coatings were formed by co-evaporation of two materials (8YSZ and Al_2O_3) in the EB-PVD chamber (Fig. 3). During co-evaporation, a partition was created between the two ingots to avoid any intermixing of the vapor cloud. The mandrel on which the sample was mounted was rotated above the

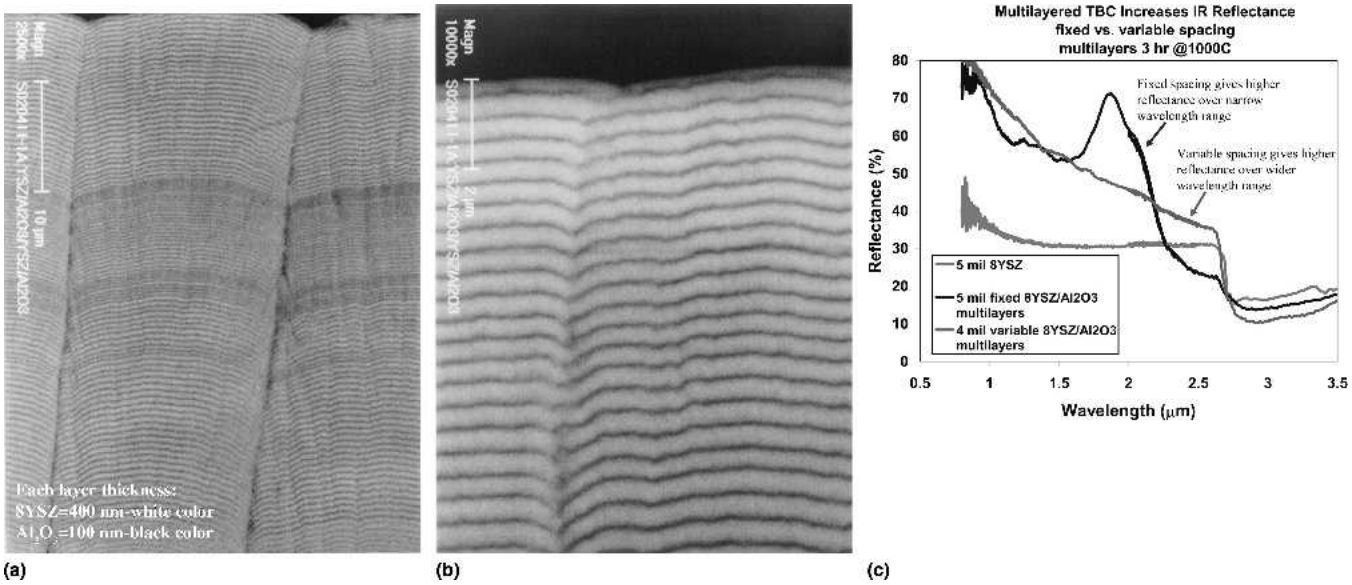

Fig. 3 (a,b) SEM photographs showing 8YSZ (white color)/Al_2O_3 (black color) nanolayered coating, and (c) hemispherical reflectance of 8YSZ/Al_2O_3 deposited by co-evaporation EB-PVD to get the desired thickness of each layer. The thickness of each Al_2O_3 layer was varied from ~75 to 100 nm (black color), whereas the thickness of 8YSZ remained constant at 400 nm (white color), as shown in (a) and (b). The corresponding hemispherical reflectance of the coating is displayed in (c).The reflectance of the coating varied from 75 to 50% over the wavelength of interest. This preliminary experiment clearly showed that the reflectance of the coatings can be tailored to achieve high reflectance over a wide wavelength range by controlling (altering) the thickness of each Al_2O_3 and 8YSZ layer.

partitioning. The rotation speed and evaporation rate of each ingot was controlled

3.6 Functionally Graded Materials

Functionally graded (FG) structural materials are gaining importance in the field of high-temperature applications, where coefficient of thermal expansion (CTE) between different materials is one of the largest concerns. Application of FG structural materials is unlimited ranging from NASA's space rocket engines to nuclear propulsion systems, high-temperature radiators, and x-ray targets. Selection of materials for forming FG structural materials is based upon the application (Ref 53-55). NASA's space rocket engine is generally made of copper-based alloys (Cu-5%Ag-0.5%Zr or Cu-8%Cr-4%Nb), which offer excellent high-temperature thermal conductivity and mechanical properties for such applications (Ref 52). The typical space rocket engine configuration (Fig. 4) consists of many cooling channels through which liquid hydrogen or oxygen is passed, maintaining the temperature well below 178 K. In the interior section of the rocket engine, the environment is extreme where liquid fuel, i.e., hydrogen and oxygen, combines in the combustion zone, resulting in very intense heat with temperatures reaching 800-900 °C. The combustion chamber liner often degrades due to oxidation of copper and thus need environmental protection coatings. Applying ceramic thermal protection coatings (such as 8YSZ) on the interior of the combustion chamber liner to minimize heat transfer to the copper liner without degrading its thermal conducting properties has been considered. One approach, which is being considered, is to apply a thin metallic coating as a bond coat such as MCrAlY (where M = Ni, Fe, Co, or mixed combination) on the Cu-liner before applying 8YSZ. The MCrAlY material was selected as it offers excellent metallurgical bonding between the MCrAlY and ZrO_2-8wt.%Y_2O_3 and also acts as a diffusion barrier for protecting copper from oxygen. The biggest challenge is in having a minimum CTE mismatch between Cu (17×10^{-6} K^{-1}), MCrAlY (15×10^{-6} K^{-1}), and 8YSZ (8.9 to 10.6 $\times 10^{-6}$ K^{-1}) without having a sharp interface, which can be achieved only by forming a functional graded coating with a smooth compositional transition from Cu → MCrAlY → ZrO_2-8 wt.%Y_2O_3. Proof of concept was demonstrated between MCrAlY and YSZ (Fig. 4) formed by EB-PVD through coevaporation of MCrAlY and YSZ. The functional graded structure was formed between the MCrAlY and ZrO_2-8wt.%Y_2O_3 in which, during the co-evaporation period, the evaporation rate of MCrAlY was decreased and evaporation rate of ZrO_2-8wt.%Y_2O_3 was increased resulting in FG zone (Fig. 4b-4c). The deposition was continued with only YSZ being evaporated to form a top layer composed only of the ceramic coating, i.e., ZrO_2-8wt.%Y_2O_3. Future efforts would entail applying a layer of copper coating followed by co-evaporation of copper and MCrAlY on the combustion chamber liner to achieve good metallurgical bonding with the base material.

3.7 Functional Graded Re → ReHf → Hf → HfN and Re → ReZr → Zr → ZrN Coatings

A similar research effort was undertaken in applying HfN and ZrN coatings as a diffusion barrier on ReMo-based alloy substrate for high-temperature applications. One such application is for lightweight heat pipe cooled leading edges with high heat flux capabilities, where refractory metal tubes embedded in the refractory composite structure serve as the containers for liquid-metal heat pipe for space application (Ref 56). Refractory metals are used because they exhibit high melting points and high strengths at elevated temperatures. They can also withstand high processing temperatures required for manufacturing refractory-composite materials. One of the complications encountered with embedding a refractory metal tube in a

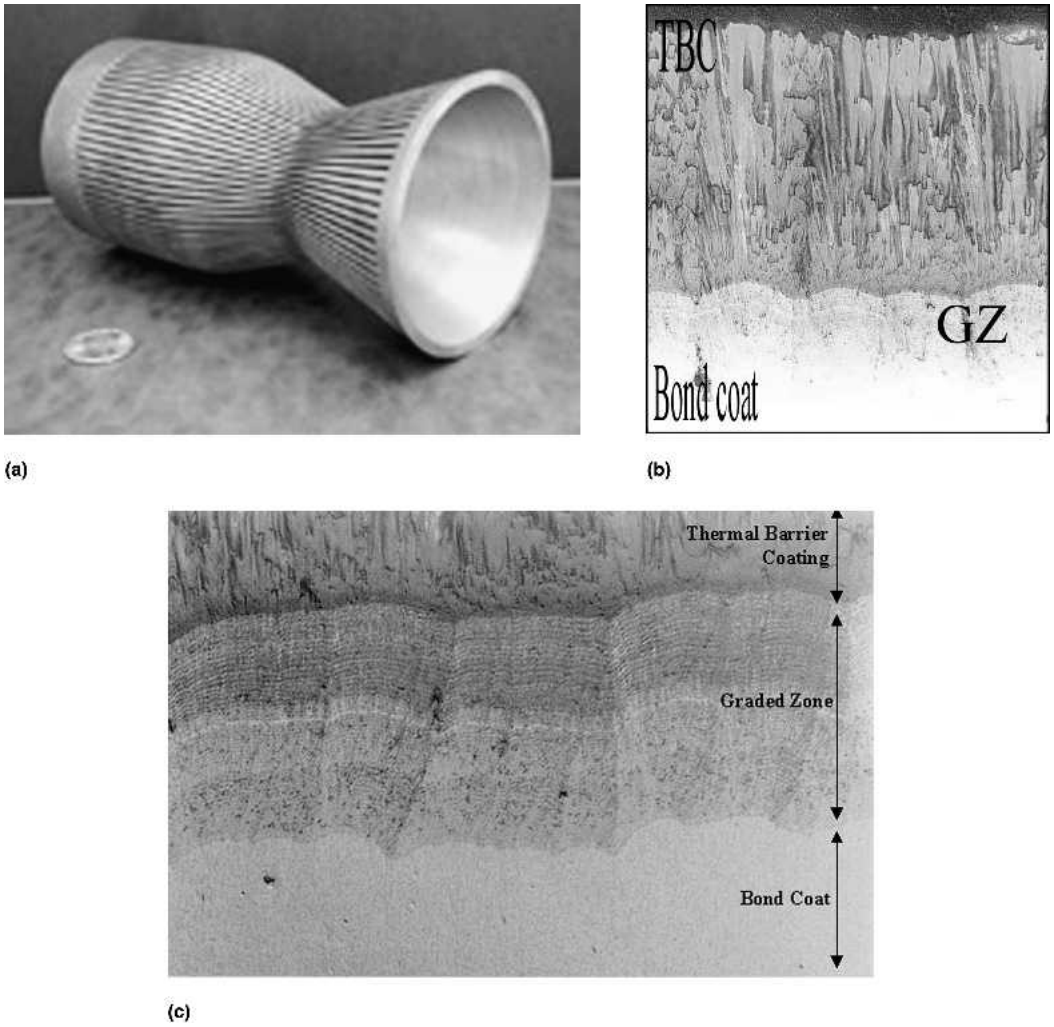

Fig. 4 (a) NASA's main combustion chamber made of copper-based alloys with cooling channels, and (b,c) cross-sectional optical micrographs showing microstructure of bond coat (MCrAlY), graded zone (GZ), and ceramic coatings (ZrO2-8wt.%Y_2O_3) produced by EB-PVD

refractory composite structure is lack of chemical compatibility between the two materials. Many refractory metals form carbides or silicides when in contact with carbon or silicon at elevated temperatures. The formation of carbide and silicides can lower the strength and ductility of the refractory metals. In addition, for heat pipe applications, carbon or silicon may diffuse through the metal tube (i.e., heat-pipe container) and contaminate the heat pipe. To minimize chemical interaction between the refractory metal heat pipe tube and refractory composite structure, various barrier coatings are being considered. Two of the diffusion barrier coatings identified are HfN and ZrN. The biggest challenge was to minimize delamination of the coating during thermal cyclic exposure caused by large CTE mismatch and poor interfaces. Functionally graded Re $\rightarrow$ ReHf $\rightarrow$ Hf $\rightarrow$ HfN structure was made by ion-beam-assisted EB-PVD, as shown in Fig. 5. Here, Re was evaporated first followed by the coevaporation of Re and Hf. Concentration of Hf was continuously increased, and Re was decreased as a function of deposition time and coating buildup, resulting in the last layer enriched in Hf (100%). This Hf layer was then reacted with ionized nitrogen gas during the deposition process forming HfN. There is no distinct interface between the Hf and the HfN structure. Figure 5(a) shows the top view of the HfN coating exhibiting nano-grained microstructure. Figure 5(b) shows the cross section of the functional graded coatings (Re $\rightarrow$ ReHf $\rightarrow$ Hf $\rightarrow$ HfN). The cause is unclear for variation in the cross-section microstructure of the functional graded coating in spite of continuous evaporation of Re $\rightarrow$ Hf materials without interruption.

3.8 Precision Net-Shaped Forming Components

Refractory metals are very attractive materials for high-temperature structural and energy system applications such as solar powered rocket engines, heat exchangers, and space and missile propulsion systems. However, it is very difficult to produce precision net-shaped components made of refractory metals such as tungsten, hafnium, and rhenium with a density >95%. Typically, components are fabricated by either powder metallurgy (P/M) or CVD. Due to difficulties encountered in the P/M fabrication and shaping of refractory parts, CVD is mainly used in fabricating thin-walled, small-diameter, or complex-shaped components and also for coatings on carbon, ceramic, and metal components. However, the CVD process also has many shortcomings. For instance, rhenium deposition is obtained by passing chlorine gas through a heated chamber (at 500 °C) containing rhenium chips resulting in rhenium pentachloride ($ReCl_5$). The gaseous molecules of $ReCl_5$ decompose

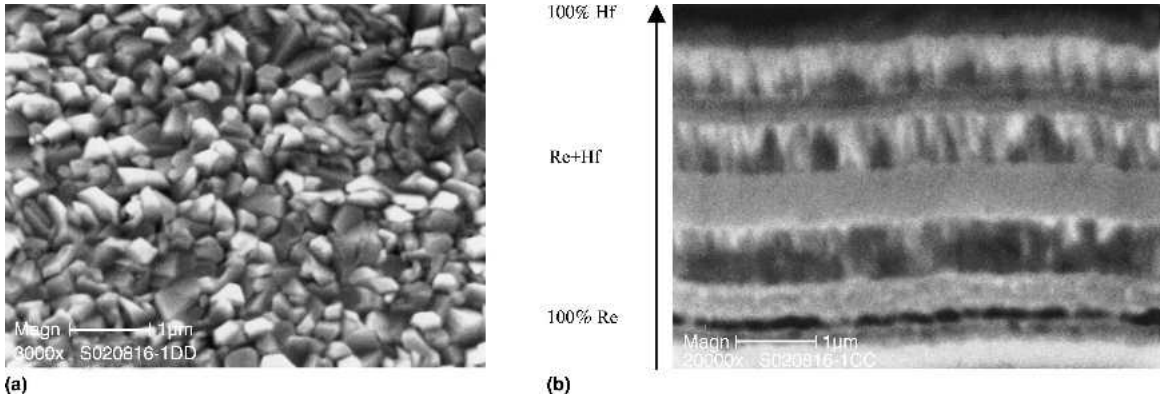

Fig. 5 (a) SEM showing the top view of the coating exhibiting nano-grained microstructure and (b) cross-section SEM showing a functionally graded ReHf material deposited on ReMo alloy plate by EB-PVD

at 1200 °C with rhenium atoms depositing on the substrate. However, CVD rhenium deposits contain entrapped gases (chlorine and hydrogen) as impurities resulting in lower physical and mechanical properties. CVD coating often produces columnar microstructure that is undesirable for structural applications. The columnar microstructure is destroyed by periodically removing partially coated components followed by mechanical grinding, i.e., partially removing rhenium-coating material and continuing recoating. This effort is repeated many times to obtain the desired thickness and density of the coating. It has been reported that the CVD rhenium substrate produced in this way exhibits multiple layers. When the CVD-Re component is heated to elevated temperature, individual layers tend to separate, allowing slippage. This phenomenon has been shown to decrease the mechanical properties of CVD-Re, which is highly undesirable for the design and incorporation of flight engines (Ref 57, 58). The second shortcoming of the CVD process is that it requires long fabrication time in producing components, and thus it is not a cost-effective manufacturing process. Because CVD is not a line-of-sight process, the interior and exterior surfaces of complex components can be coated simultaneously. However, it is difficult to apply uniform coating "thickness" on spherical components, i.e., graphite balls, due to limited flexibility in maneuvering parts in the reaction chamber, gas flow dynamics, and the entire surface area to be coated simultaneously (i.e., 360°). Depending on the dimension of the components, generally one component (such as thruster) is manufactured at a time in the CVD reactor chamber.

P/M techniques were explored in the fabrication of rhenium components (Ref 59). These techniques also have their limitations with respect to cost, speed, achievable geometry, required tooling, and high-temperature isostatic pressure (HIP) treatment for compaction (Ref 58). Various steps are involved in the manufacturing of components including cold isostatic pressing, pre-sintering at 1200 °C, and hot sintering at 2500 °C. Densities greater than 99% are achievable only after extensive, accumulated cold and hot working. Hot working of rhenium must be carried out in a hydrogen environment. In air, the rhenium metal readily oxidizes to the heptoxide (melting point 297 °C), so hot working in air is not possible. This extensive value-added processing contributes to high cost and fairly limited range of commercial shape components. Fabrication of components by powder-plasma spray process has also been explored and exhibits poor mechanical properties due to the presence of a large volume fraction of porosity. An effort was undertaken to address shortcomings of CVD and P/M techniques and identify an alternative manufacturing method in fabricating net-shaped components with density >95% in a cost-effective manner (Ref 60). Electron beam-physical vapor deposition (EB-PVD) method has met these challenges.

3.9 Fabrication of Rhenium Plate

The first effort undertaken was to demonstrate that rhenium plates produced by EB-PVD had equivalent or better physical and mechanical properties in comparison with conventional CVD process. The rhenium ingot was used as a source material that was supplied by Rhenium Alloys Inc., Elyira, OH (density 98% and purity 99.99%). A focused high-energy electron beam was used to evaporate the rhenium ingot in the coating chamber and deposited on graphite plates. During the deposition process, the graphite plates were indirectly heated up to 1000 °C. The microstructure of the coating was tailored by changing various process parameters including evaporation rate, periodically interrupting incoming vapor flux, and vapor incidence angle (VIA), as shown in Fig. 6(a) and (b) (Ref 61). A novel concept was developed to avoid any continuous columnar grain formation during deposition; i.e., the in and out approach was used in forming textured subgrain microstructure as shown in Fig. 6(c). In addition, the rhenium plate exhibited textured grain growth with micron- and submicron-sized microstructure. Coated plates exhibited higher hardness (283 VHN) than the CVD rhenium plate with hardness of 245VHN. Using the Hall-Petch equation along with the grain size and hardness, it is predicted that the Re plate will exhibit 30% improvement in mechanical properties as compared with CVD Re plate, which was confirmed by measuring mechanical properties (tensile strength of EB-PVD Re was ~72 ksi and CVD Re was ~50 ksi). Rhenium plates were found to be free from impurities such as copper or other materials. During the course of this investigation, it was demonstrated that the growth orientation of the coatings can be changed by periodically changing the vapor incidence angle (VIA) of the incoming flux, as shown in Fig. 6(c).

3.10 Fabrication of Rhenium-Coated Graphite Balls

Applying uniform rhenium coating on graphite balls (or cores) by EB-PVD is a demonstration in net-shape forming

(a)

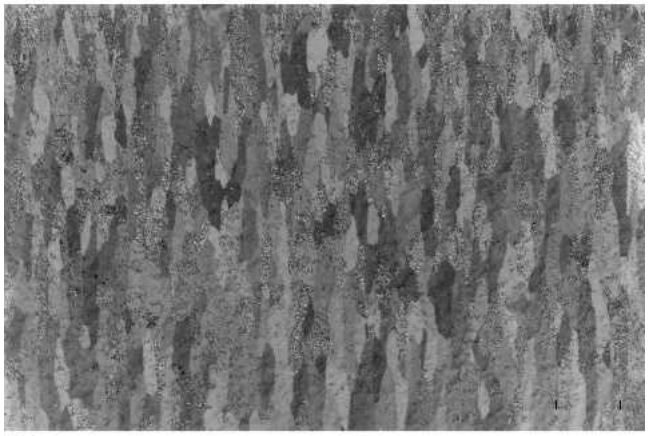

(b)

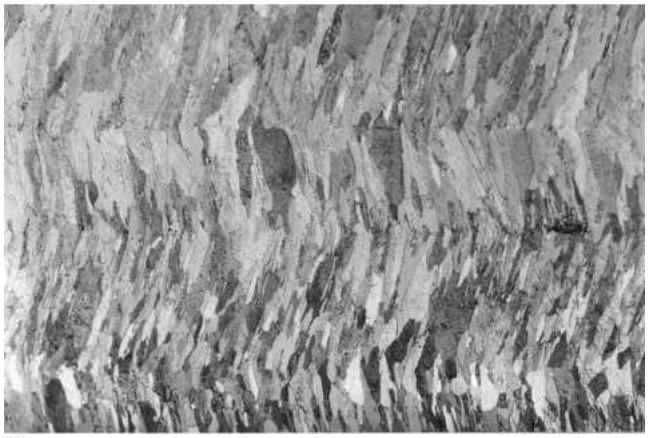

(c)

Fig. 6 (a) Optical micrograph showing (a) continuous single columnar grains, (b) textured subgrains, and (c) zig-zag microstructure of Re-plate (2000 µm) deposited on graphite produced by EB-PVD

components. Seventeen graphite cores (diameter ~15 mm) were simultaneously charged into a cylindrical cage, as shown in Fig. 7. The cage was fabricated using molybdenum wire mesh. The cylindrical cage was rotated at 7-10 rpm above the melt pool within the rhenium vapor. During the deposition process, cores were heated to 1000 °C by radiation heating under the A-frame graphite heater. The Re-coated graphite

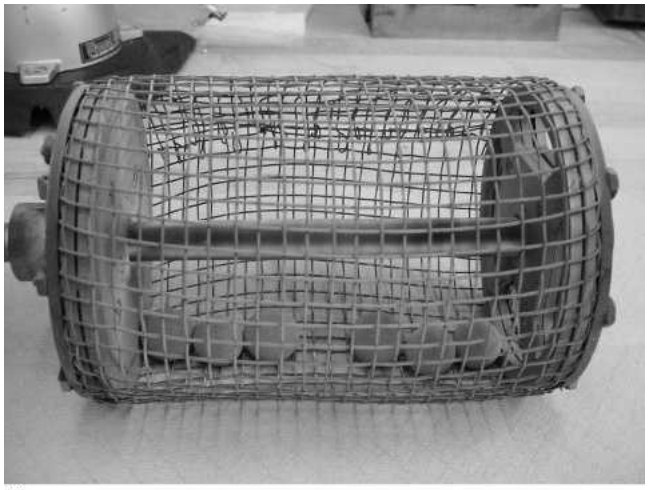

(a)

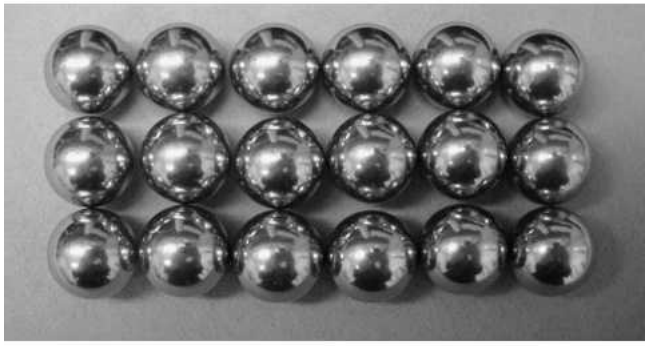

(b)

Fig. 7 (a) Mo-cage used for applying Re coatings on graphite cores and (b) polished Re-coated graphite cores with surface finish <Ra 8.

cores were also simultaneously bombarded with ionized argon gas during deposition to obtain a dense uniform microstructure. After applying rhenium to the full coating thickness, eighteen coated cores were simultaneously polished in the laboratory vibromet-polishing unit to the surface finish <Ra 8 (Fig. 7b).

All coated cores exhibited uniform coatings with 100% concentricity, which was measured by coordinate measuring machine (CMC). It is important to mention here that there are more than 250 µm and submicron grains through the coating thickness (2000 µm) with a much finer grain structure (Fig. 8).

3.11 Fabrication of Rhenium Tubes

A similar effort was undertaken in manufacturing of rhenium (Re) tubes with a wall thickness of 150 µm and length of 25 cm. Such tubes were manufactured using Mo as sacrificial mandrels on which Re was deposited. Once the Re coating is deposited, the Mo mandrel is removed by chemical dissolution, leaving behind the skin of the coating (i.e., Re in the tubular form). Currently, Re tubes are manufactured by CVD. The main drawback of this process is that the Re tube contains 2-4 grains through the wall thickness, which does not provide adequate number of grains for welding and bending applications (Fig. 9c). In addition, there are not enough grains through the wall thickness to accommodate pressure under high-temperature burst tests. Again, CVD process is limited in

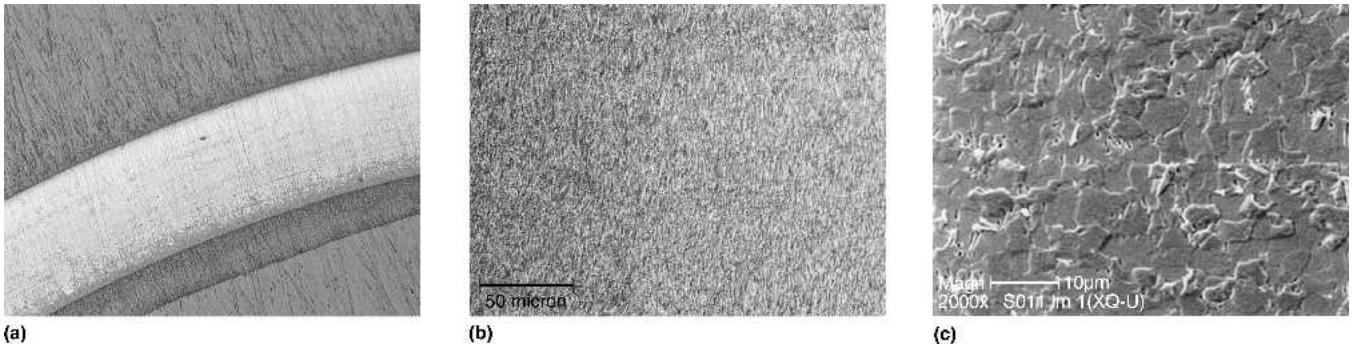

Fig. 8 Cross section of the rhenium-coated graphite core exhibiting dense microstructure with nano- and submicron-sized grains: (a) optical micrograph low magnification, (b) optical micrograph high magnification, and (c) SEM micrograph.

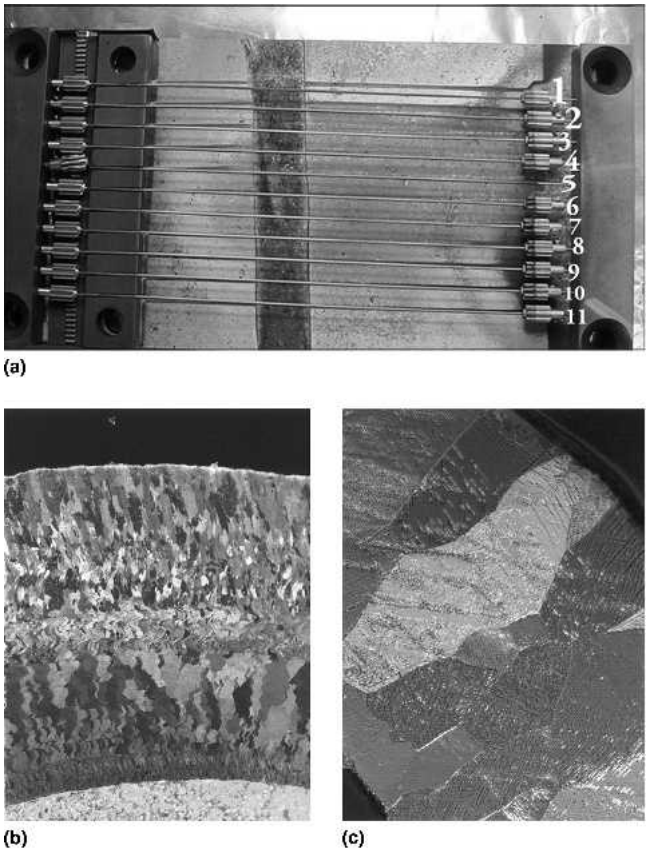

Fig. 9 (a) Tube tooling, optical micrograph, (b) cross section of Re tube produced by EB-PVD exhibiting >40-50 grains throughout the 150 μm wall thickness, and (c) cross section of Re tube produced by CVD exhibiting 1-3 grains through 150 μm wall thickness for comparison

manufacturing of Re tubes (2-3 tubes at a time). The shortcoming of CVD process was addressed by exploiting EB-PVD technology. Similarly, Mo mandrel concept was used in manufacturing of Re tubes by ion beam assisted (IBA), EB-PVD. Tooling concept developed in the manufacturing of Re tube by EB-PVD is displayed in Fig. 9(a). Eleven Mo mandrels were mounted simultaneously for applying Re coatings. Mo mandrels were periodically rotated to get uniform coating thickness across the diameter. Mo mandrels were heated indirectly to 1000 °C during Re deposition. The cross section of the rhenium-coated Mo mandrel is shown in Fig. 9(b). Rhenium coating was very uniform around the Mo tube. Optical microstructure of the coated tube exhibited more than 40-50 grains through the wall thickness that is 10 times more grains than the current CVD process, i.e., nano-grained and submicron grained microstructure was observed through the rhenium wall thickness.

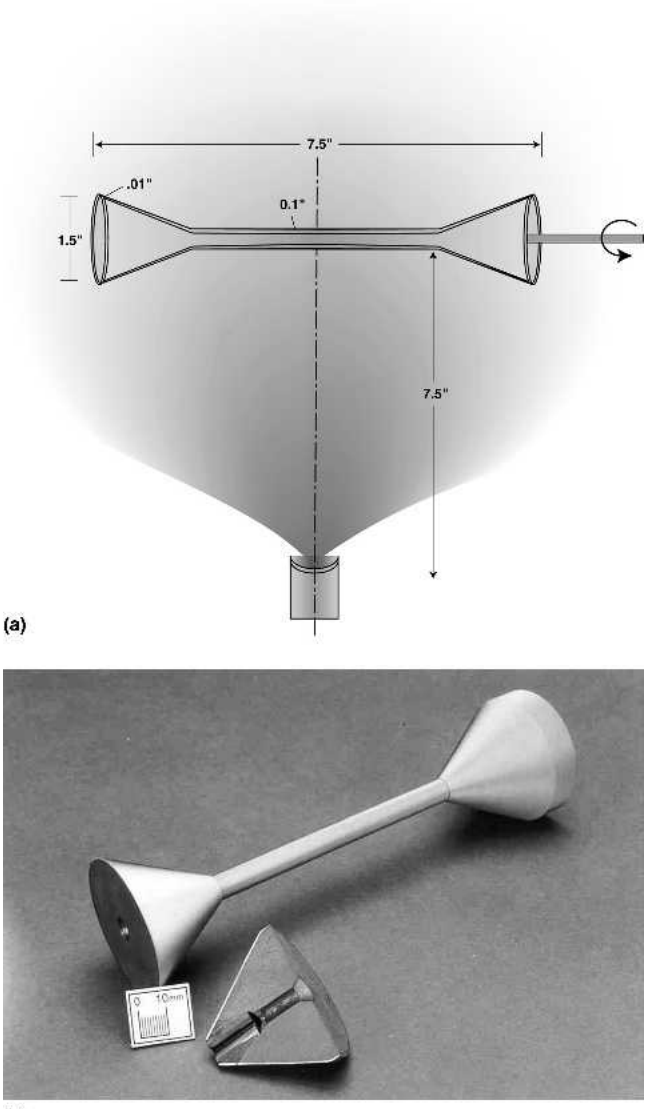

Fig. 10 (a) Diagram showing fabrication of two thrusters simultaneously and (b) two mirror images of titanium-coated graphite mandrel thrusters by EB-PVD with cross section

3.12 Fabrication of Net-Shaped Thruster

Net-shaped thruster fabrication was demonstrated using titanium as an evaporant due to the high cost of rhenium. The high flexibility of the EB-PVD process, allowed two thrusters (mirror image) to be fabricated simultaneously during the deposition process (Fig. 10a and b). In contrast, the rhenium thruster is currently made by the CVD process, and only one thruster is made at a time due to the limited flexibility in the chamber.

4. Summary

This review article demonstrated the versatility of EB-PVD from nano-flakes, coatings, net-shaped forming components. Sequential or simultaneous co-evaporation of multiple ingots allowed engineering of new coating materials, forming functional graded coatings, components with superior properties including mechanical (hardness and strength), and physical properties such as thermal conductivity and thermal reflectance. Attachment of an ion source to the EB-PVD unit offers additional benefits and flexibility in depositing textured high-density coatings at a relatively low temperature. Processing parameters control the microstructure, physical and mechanical properties, and residual stresses present within the coating.

References

1. J. Sobota, G. Sorensen, H. Jensen, Z. Bochnicek, and V. Holy, C-N/MeN Nanocomposite Coatings, Deposition and Testing of Performance, *Surf. Coat. Technol.,* Vol 142-144, 2001, p 590-595
2. K.C. Chin, A. Gohel, H.I. Elim, W.Ji, G.L. Chong, K.Y. Lim, C.H. Sow, and A.T. S. Wee, Optical Limiting Properties of Amorphous Si_xN_y and SiC Coated Carbon Nanotubes, *Chem. Phy. Lett.,* Vol 383 (No. 1-2), 2004, p 72-75
3. M. Brogren, G.L. Harding, R. Karmhag, C.G. Ribbing, G.A. Niklasson, and L. Stenmark, Titanium-Aluminum-Nitride Coatings for Satellite Temperature Control, *Thin Solid Films,* Vol 370 (No. 1-2,) 2000, p 268-277
4. Q. Xiang, Y. Zhou, B.S. Ooi, Y.L. Lam, Y.C. Chan, and C.H. Kam, Optical Properties of Er^{3+}-doped SiO_2-GeO_2-Al_2O_3 Planar Waveguide Fabricated by Sol-Gel Processes, *Thin Solid Films,* Vol 370 (No. 1-2), 2000, p 243-247
5. H. Holleck, Design of Nanostructured Thin Films for Tribological Applications, *TMS Conference Proceedings on Surface Engineering: Science and Technology I,* A. Kumar, Y.W. Chung, J.J. Moore, and J.E. Smugeresky, Ed., Minerals, Metals, and Materials Society, Warrendale, PA, 1999, p 207
6. R.A. Miller, "Thermal Barrier Coatings for Aircraft Engines—History and Directions," Thermal Barrier Coating Workshop, NASA CP 3312, 1995, p 17
7. O. Unal, T.E. Mitchell, and A.H. Heuer, Microstructures of Y_2O_3-Stabilized ZrO_2 Electron Beam-Physical Vapor Deposition Coatings on Ni-Base Superalloys, *J. Am. Ceram. Soc.,* Vol 77 (No.4), 1994, p 984-992
8. R.A. Miller, Current Status of Thermal Barrier Coatings—An Overview, *Surf. Coat. Technol.,* Vol 30, 1987, p 1
9. J. Singh, D.E. Wolfe, and J. Singh, Architecture of Thermal Barrier Coatings Produced by Electron Beam-Physical Vapor Deposition (EB-PVD), *J. Mater. Sci.,* Vol 37, 2002, p 3261-3267
10. K.L. Choy, Chemical Vapor Deposition of Coatings, *Prog. Mater. Sci.,* Vol 48 (No. 2), 2003, p 57-170
11. D.E. Wolfe, "Growth of Titanium Nitride Coatings by Reactive Ion Beam-Assisted, Electron Beam-Physical Vapor Deposition (RIBA, EB-PVD) and Hard Coatings Evaluation," Thesis 1996 MSWolfe DE, Penn State University, University Park, PA, 1996
12. *Handbook of Deposition Technologies for Films and Coatings,* R. Bunshah, Ed., Noyes Publications, Park Ridge, NJ, 1994
13. M. Hocking, *Metallic and Ceramic Coatings, Longman Scientific and Technical,* John Wiley and Sons Inc., 1989
14. *Physical Vapor Deposition,* R.J. Hill, Ed., Temescal, a division of the BOC Group, Inc., Berkeley, CA, 1986, p 1-85
15. R. McIntyre, *Mater. Process.,* Vol 8, 1996, p 455
16. J. Singh, Laser Beam and Photon-Assisted Processed Materials and Their Microstructure, *J. Mater. Sci.,* Vol 29, 1994, p 5232-5258
17. Y-J. Tan and K.Y. Lim, Understanding and Improving the Uniformity of Electrodeposition, *Surf. Coat. Technol.,* Vol 167 (No. 2-3), 2003, p 255-262
18. S.S. Eskildsen, C. Mathiasen, and M. Foss, Plasma CVD: Process Capabilities and Economic Aspects, *Surf. Coat. Technol.,* Vol 116-119, 1999, p 18-24
19. W. Beele, G. Marijnissen, and A. Van Lieshout, The Evolution of Thermal Barrier Coatings—Status and Upcoming Solutions for Today's Key Issues, *Surf. Coat. Technol.,* Vol 120-121, 1999, p 61-67
20. P. Fauchais and A. Vardelle, Heat, Mass and Momentum Transfer in Coating Formation by Plasma Spraying, *Int. J. Therm. Sci.,* Vol 39 (No. 9-11), 2000, p 852-870
21. D.E. Wolfe and J. Singh, Functionally Gradient Ceramic/Metallic Coatings for Gas Turbine Components by High-Energy Beams for High-Temperature Applications, *J. Mater. Sci*., Vol 33, 1998, p 3677-3692
22. D.E. Wolfe, M. Movchan, and J. Singh, Architecture of Functionally Graded Ceramic Metallic Coatings by Electron Beam-Physical Vapor Deposition, *Proceeding of Advances in Coating Technologies,* TMS Annual Meeting at Orlando, C.R. Clayton and J.K. Hirvonen, Ed., TMS, Warrendale, PA, 1997, p 93
23. D.E. Wolfe J. Singh, and K. Narasimhan, Synthesis and Characterization of Multilayered TiC/TiB2 Coatings Deposited by Ion Beam Assisted, Electron Beam-Physical Vapor Deposition (EB-PVD), *J. Surf. Coat. Technol.,* Vol 165, 2003, p 8-25
24. D.E. Wolfe, "Synthesis and Characterization of TiC, TiBCN, TiB2/TiC, and TiC/CrC Multilayer Coatings by Reactive and Ion Beam Assisted, Electron Beam-Physical Vapor Deposition (EB-PVD)," Thesis 2001D Wolfe DE, Penn State University, University Park, PA, 2001
25. J.L. Vossen and J.J. Cuomo, *Thin Film Process,* Academic Press, Inc., 1978, p 11-73
26. W. Ensinger, A. Schroer, and G.K. Wolf, A Comparison of IBAD-Films for Wear and Corrosion Protection with Other PVD-Coatings, *Nucl. Instrum. Meth. Phys. Res. B,* Vol 80/81, 1993, p 445-454
27. J. Arnalt, J. Delafond, C. Templier, J. Chaumont, and O. Enea, First Stages Study of High Energy Ion Beam Assisted Deposition, *Nucl. Instrum. Meth. Phys. Res. B*, Vol 80/81, 1993, p 1384-1387
28. J. Hirvonen, Ion Beam Assisted Thin Film Deposition, *Mater. Sci. Rep.,* Vol 6, 1991, p 215-274
29. H. Kaufman, R.S. Robinson, and W.E. Hughes, *Characteristics, Capabilities, and Applications of Broad-Beam Sources,* Commonwealth Scientific Corporation, Alexandria, VA, 1987, p 1-38
30. H. Oettel and R. Wiedemann, Residual Stresses in PVD Hard Coatings, *Surf. Coat. Technol.,* Vol 76-77, 1995, p 265-273
31. I.C. Noyan, T.C. Huang, and B.R. York, Residual Stress/Strain Analysis in Thin Films by X-ray Diffraction, *Crit. Rev. Solid State Mater. Sci.,* Vol 20 (No. 2), 1995, p 125-177
32. A. Peiter and H. Wern, Residual Stresses, *Strain,* August, 1987, p 103-107
33. R. Hull, J.C. Bean, F. Ross, D. Bahnck, and L.J. Peticolas, The Roles of Stress, Geometry and Orientation on Misfit Dislocation Kinetics and Energetics in Epitaxial Strained Layers, *Mater. Res. Soc. Symp. Proc.,* Vol 239, 1992, p 379-395
34. J.H. Je, D.Y. Noh, and K.S. Liang, Preferred Orientation of TiN Films Studied by a Real Time Synchrotron X-Ray Scattering, *J. Appl. Phys.,* Vol 81 (No. 9), 1997, p 6126-6133
35. G. Knuyt, C. Quaeyhaegens, J. D'Haen, and L.M. Stals, A Quantitative Model for the Evolution From Random Orientation to a Unique Texture in PVD Thin Film Growth, *Thin Solid Films,* Vol 258, 1995, p 159-169
36. B. Rauschenbach and K. Helming, *Nucl. Instrum. Meth. Phys. Res. B,* Vol 42, 1989, p 216-223
37. T. Roth, K.H. Kloos, and E. Broszeit, Structure, Internal Stresses, Adhesion, and Wear Resistance of Sputtered Alumina Coatings, *Thin Solid Films,* Vol 153, 1987, p 123-133
38. F.A. Quli, "Molybdenum Metallization and Step-Induced Defects in Active Matrix Liquid Crystal Displays," Thesis 1999d Quli FA, Penn State University, University Park, PA, 1999
39. D.E. Wolfe and J. Singh, Microstructural Evolution of Titanium Nitride (TiN) Coatings Produced by Reactive Ion Beam-Assisted, Elec-

tron Beam Physical Vapor Deposition, *J. Mater. Sci.,* Vol 34, 1999, p 2997-3006
40. W. Sproul, PVD Today, *Cutting Tool Eng.,* February 1994, p 52-57
41. H. Holleck, M. Lahres, and P. Woll, Multilayer Coatings—Influence of Fabrication Parameters on Constitution and Properties, *Surf. Coat. Technol.,* Vol 41, 1990, p 179-190
42. D.E. Wolfe and J. Singh, Synthesis and Characterization of TiBCN Coatings Deposited by Ion Beam Assisted, Co-Evaporation Electron Beam-Physical Vapor Deposition (EB-PVD), *J. Mater. Sci.,* Vol 37, 2002, p 3777-3787
43. D.E. Wolfe and J. Singh, Titanium Carbide Coatings Deposited by Reactive Ion Beam-Assisted Electron Beam—Physical Vapor Deposition, *Surf. Coat. Technol.,* Vol 124, 2000, p 142-153
44. D.E. Wolfe, J. Singh, and K. Narasimhan, Synthesis of Titanium Carbide/Chromium Carbide Multilayers by the Co-Evaporation of Multiple Ingots by Electron Beam Physical Vapor Deposition, *Surf. Coat. Technol.,* Vol 160, 2002, p 206-218
45. D.E. Wolfe and J. Singh, Functionally Graded Ceramic Metallic Coatings for Gas Turbine Components by High-Energy Beams for High-Temperature Applications, NATO-Advanced Study Institute Series Proceedings: Protective Coatings and Thin Films, Y. Pauleau and P. Barna, Ed., Kluwer Academic Publishers, Dordrecht, The Netherlands, Vol 21, 1996, p 441-465
46. D.E. Wolfe and J. Singh, Metallurgical Evaluation and Recommendation of Hard Coatings for Cutting Tool Life Enhancement, Technical Memorandum 97, Applied Research Laboratory, Penn State University, State College, PA, February 1996
47. J. Singh, Thermal Barrier Coatings (TBC) by Electron Beam-Physical Vapor Deposition (EB-PVD) Process, *Surf. Eng. Bull.,* Vol 7, 1996, p 8
48. B.C. Oberlander and E. Lugscheider, *Mater. Sci. Technol.,* Vol 9, 1992, p 657
49. R.A. Miller, *Surf. Coat. Technol.,* Vol 309, 1987, p 1-11
50. K.S. Ravichanaran, K. An, R.E. Dotton, and S.L. Semiatin, *J. Am. Ceram. Soc.,* Vol 82 (No. 30), 1999, p 673-682
51. J. Singh, D.E. Wolfe, R. Miller, J. Eldridge, and D-M. Zhu, Thermal Conductivity and Thermal Stability of Zirconia and Hafnia Based Thermal Barrier Coatings by EB-PVD for High Temperature Applications, II International Materials Symposium, Universidade Nova de Lisboa, Campus da Caparica, Portugal, April 14-16, 2003.
52. D.E. Wolfe, J. Singh, R. Miller, J. Eldridge, and D. Zhu, Tailored Microstructure of EB-PVD 8YSZ Thermal Barrier Coatings With Low Thermal Conductivity and High Thermal Reflectivity for Turbine Applications, *Surf. Coat. Technol.,* Vol 190, 2005, p 132-149
53. D.V. Rigney, R. Viguie, D.J. Wartman, and D.W. Skelly, PVD Thermal Barrier Coating Applications and Process Development for Aircraft Engines, *J. Therm. Spray Technol.,* Vol 6, 1997, p 167
54. U. Schultz, T. Krell, U. Leushake, and M. Peters, Graded Design of EB-PVD TBC System, Proc. AGARD Workshop on Thermal Barrier Coatings, Aalborg, DK, October 15-16, 1997
55. Yong-ho Sohn, "Characterization and Life Prediction of Physical Vapor Deposited Partially Stabilized Zirconia Thermal Barrier Coatings," Ph.D. Thesis, Worcester Polytechnic Institute, MA, 1993
56. D.E. Glass, R.N. Shenoy, Z. Wang, and M. Halbig, "Effectiveness of Diffusion Barrier Coatings for Mo-Re Embedded in C/SiC and C/C," NASA/TM, 2001, p 1264
57. A.J. Sherman, R.H. Tuffias, and R.B. Kaplan, The Properties and Applications of Rhenium Produced by CVD, *J. Metals,* July 1991, p 20-23
58. B.D. Reed, J.A. Biaglow, and S. Schneider, "Iridium–coated Rhenium Radiation Cooled Rockets," NASA Technical Memorandum Number 107453, 1997, p 1-13
59. T. Leonhardt, M. Hamister, J. Carlen, J. Biaglow, and B. Reed, Near Net Shape Powder Metallurgy Rhenium Thruster, in *Conference Proceedings of 36th American Institute of Aeronautics,* Reston, VA (17–19 July 2000), p 1-11
60. J.O. Milewski, D.J. Thoma, J.C. Fonseca, and G.K. Lewis, Directed Light Fabrication of Rhenium Components, *Mater. Manuf. Process.,* Vol 13, 1998, p 719-730
61. J. Singh and D.E. Wolfe, Net-Shape Rhenium Fabrication by EB-PVD, *J. Adv. Mater. Process.,* Vol 160, 2002, p 39-42